Available online at www.sciencedirect.com
SCIENCE DIRECT®
Journal of Sound and Vibration 282 (2005) 1293–1307
JOURNAL OF SOUND AND VIBRATION
www.elsevier.com/locate/jsvi

Short Communication

Integrated optimal design of vibration control system for smart beams using genetic algorithms

Yaowen Yang*, Zhanli Jin, Chee Kiong Soh

Division of Structures and Mechanics, School of Civil & Environmental Engineering, Nanyang Technological University, Nanyang Avenue 50, Singapore 639798, Singapore

Received 15 December 2003; accepted 15 March 2004
Available online 14 October 2004

Abstract

In this paper, the parameters of vibration control system of smart beams, including the placement and size of piezoelectric sensors and actuators (S/As) bonded on smart beams and the feedback control gains of the control system, have been simultaneously optimized for vibration suppression of beam structures. Since the sizes of the S/As are selected from a prescribed patch pool provided by the manufactures, the size design variable is then discrete, but the locations and feedback gains are continuous. Thus, the resulting optimization problem has discrete-continuous design variables which is difficult for the conventional optimization methods to solve. An integer-real-encoded genetic algorithm has thus been developed to search for the optimal placement and size of the piezoelectric patches as well as the optimal feedback control gains. The criterion based on the maximization of energy dissipation was adopted for the optimization of the control system. The optimal distributions of the piezoelectric patches based on specific controlled vibration modes have also been addressed. The results showed that the control effect could be significantly enhanced with appropriate distribution of piezoelectric patches and selection of feedback control gains, and meaningful observations have been obtained for practical design.

*Corresponding author. Tel.: +65-67906-227; fax: +65-679-106-76.
E-mail address: cywyang@ntu.edu.sg (Y. Yang).

0022-460X/$ - see front matter © 2004 Elsevier Ltd. All rights reserved.
doi:10.1016/j.jsv.2004.03.048

1. Introduction

Vibration control of flexible structures has been a major research topic over the past few decades. In recent years, a great number of research results have been produced in active structural vibration control using piezoelectric materials as distributed sensors and actuators (S/As). The piezoelectric S/As have to be of suitable size and be appropriately located to ensure the maximum effectiveness for optimal vibration control.

In recent years, efforts have been mainly concentrated on finding the optimal size and location of the S/As. Crawley and de Luis [1] were the first to address the criterion for finding the optimal location of a piezoelectric actuator for a cantilever beam. Baz and Poh [2] solved the problem of location optimization of an actuator with pre-selected size. Devasia et al. [3] considered the problem of placement and sizing optimization of distributed piezoelectric actuators on a uniform beam. Dhingra and Lee [4] addressed the influence of S/A locations and feedback gains on the optimum design of actively controlled structures. For the case of optimization of actuator location, different cost functions and performance measures have been used. Some researchers [5,6] proposed to maximize the controllability criterion using a measure of the gramian matrix. A quadratic cost function taking into account the measurement error and control energy has also been proposed [7,8]. As can be found from the available literature, most attention has been paid on the geometric optimization of S/As such as their placement, size as well as thickness; but integrated control system optimization considering the placement and size of the piezoelectric patches and the feedback control gains of the control system has rarely been investigated.

In this study, the geometric distribution of the piezoelectric patches including the placement and size, and the feedback control gains of the actuators, have been simultaneously optimized to achieve the goal of optimal vibration suppression. The energy dissipation method [9] has been adopted as the criterion for the optimization of the control system based on the maximization of dissipation energy due to the control action. Furthermore, the optimal distribution of the piezoelectric patches based on different controlled vibration modes has also been addressed.

Recently, genetic algorithms (GAs) as an optimization technique have been applied to this kind of optimization problems [10–12]. Much effort has been concentrated on finding the optimal size and placement of the piezoelectric patches, but most of them prescribed the amount and size of the piezoelectric patches in advance while trying to optimize the placement. The integrated size and placement optimization as well as the feedback control gains has seldom been carried out.

In this study, the locations of S/As and feedback gains are defined as continuous variables, while the sizes of S/As are selected from a prescribed patch pool which includes a series of standard patches provided by the manufacturers, implying that the size design variable is discrete. Thus, the resulting optimization problem has discrete and continuous design variables, which is difficult for the conventional optimization methods to solve. Therefore, an integer–real-encoded GA has been developed to solve this problem. A simply supported beam has been exemplified to demonstrate the feasibility of this method and the effectiveness of vibration suppression. The results showed that the control effect could be significantly enhanced with appropriate distribution of piezoelectric patches and selection of feedback control gains. Furthermore, some heuristic observations have been obtained for practical design.

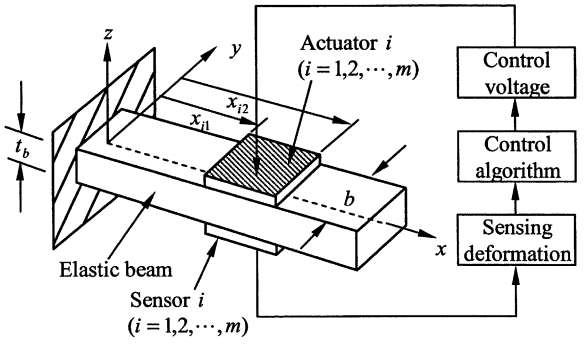

Fig. 1. Beam model with sensors and actuators.

2. Modeling of sensing and actuating

Consider a beam model, as shown in Fig. 1, bonded with piezoelectric actuators on the upper surface and sensors on the lower surface. It is well known that collocated sensors and actuators are advantageous from the viewpoint of stability; hence in this study, collocated S/As are considered. Assume that m pieces of collocated S/As are bonded on the beam. The piezoelectric material is supposed to be transversely isotropic and polarized in the z direction.

When external charges are exerted on the piezoelectric actuators, the motion equation of the beam can be expressed as [13]

$$E_b J_b \frac{\partial^4 w}{\partial x^4} + \rho_b A_b \frac{\partial^2 w}{\partial t^2} - b \sum_{i=1}^{m} \frac{\partial^2 M_i^a}{\partial x^2} = 0, \tag{1}$$

where w is the deflection of the beam; E_b, J_b, ρ_b, b and A_b are Young's modulus, inertia moment, density, width and cross-sectional area of the beam, respectively; and M_i^a is the force moment induced by actuator i, which can be written as

$$M_i^a = r^a d_{31} E_p \phi_i^a(x,t), \tag{2}$$

where d_{31} and E_p are the piezoelectric strain constant and Young's modulus of the actuators, respectively; $\phi_i^a(x,t)$ is the voltage applied to actuator i; and r^a denotes the distance measured from the neutral surface of the beam to the mid-plane of the actuator.

The voltage distribution of actuator i can be expressed as

$$\phi_i^a(x,t) = \phi_i^a(t)[H(x - x_{i1}) - H(x - x_{i2})], \tag{3}$$

in which $H(\cdot)$ is the Heaviside step function; and x_{i1}, x_{i2} are the coordinates of the two ends of actuator i.

Using the modal decomposition method and truncating the modes at n, the deflection w of the beam can be written as

$$w(x,t) = \sum_{j=1}^{n} U_j(x)\eta_j(t), \tag{4}$$

where $U_j(x)$ is the normalized orthogonal modal shapes and $\eta_j(t)$ is the modal amplitudes.

Substituting Eqs. (2)–(4) into Eq. (1) and projecting onto the jth mode yield the following equation:

$$\ddot{\eta}_j(t) + \omega_j^2 \eta_j(t) = K_a[U_j'(x_{i2}) - U_j'(x_{i1})]\phi_i^a(t) \quad (j = 1, 2, \ldots, n), \tag{5}$$

where ω_j is the natural frequency which can be expressed as $\omega_j^2 = \int_0^L E_b J_b U_j'' U_j'' \mathrm{d}x$; L is the length of the beam; $K_a = br^a d_{31} E_p$; and the prime($'$) indicates the gradient of the function.

When the beam deforms, the average output voltage ϕ_i^s over the ith sensor with an effective electrode surface S^e can be calculated as

$$\phi_i^s = -\frac{bh^s}{S^e} \int_{x_{i1}}^{x_{i2}} \left(h_{31} r^s \frac{\partial^2 w}{\partial x^2} \right) \mathrm{d}x = K_s \sum_{j=1}^{n} [U_j'(x_{i2}) - U_j'(x_{i1})]\eta_j(t), \tag{6}$$

where $K_s = -[h^s/(x_{i2} - x_{i1})]h_{31} r^s$; h^s is the thickness of the sensor, h_{31} is the piezoelectric constant, and r^s denotes the distance measured from the neutral surface of the beam to the mid-surface of the sensor.

Introducing state vector $\boldsymbol{\chi} = [\eta_1, \eta_2, \ldots, \eta_n, \dot{\eta}_1, \dot{\eta}_2, \ldots, \dot{\eta}_n]^{\mathrm{T}}$, the vibration and sensing equations, i.e., Eqs. (5) and (6), can be transformed into

$$\begin{aligned} \dot{\boldsymbol{\chi}} &= \overline{\mathbf{A}}\boldsymbol{\chi} + \overline{\mathbf{B}}\boldsymbol{\phi}_a, \\ \boldsymbol{\phi}_s &= \overline{\mathbf{C}}\boldsymbol{\chi}, \end{aligned} \tag{7}$$

in which the structural damping is included and

$$\overline{\mathbf{B}} = \begin{bmatrix} \mathbf{0}_{n\times m} \\ \tilde{\mathbf{B}} \end{bmatrix}, \quad \overline{\mathbf{C}} = [\tilde{\mathbf{C}} \quad \mathbf{0}_{m\times n}], \tag{8}$$

$$\tilde{\mathbf{B}} = \begin{bmatrix} B_{11} & B_{12} & \ldots & B_{1m} \\ B_{21} & B_{22} & \ldots & B_{2m} \\ & & \vdots & \\ B_{n1} & B_{n2} & \ldots & B_{nm} \end{bmatrix}, \quad \tilde{\mathbf{C}} = \begin{bmatrix} C_{11} & C_{12} & & C_{1n} \\ C_{21} & C_{22} & \ldots & C_{2n} \\ \vdots & \vdots & & \vdots \\ C_{m1} & C_{m2} & & C_{mn} \end{bmatrix}, \tag{9}$$

$$B_{ji} = K_a[U_j'(x_{i2}) - U_j'(x_{i1})], \quad C_{ij} = K_s[U_j'(x_{i2}) - U_j'(x_{i1})], \tag{10}$$

$$\overline{\mathbf{A}} = \begin{bmatrix} \mathbf{0}_{n\times n} & \mathbf{I}_{n\times n} \\ -\boldsymbol{\Omega}^2 & -2\boldsymbol{\varsigma}\boldsymbol{\Omega} \end{bmatrix}, \quad \boldsymbol{\phi}_a = \begin{bmatrix} \phi_1^a \\ \phi_2^a \\ \vdots \\ \phi_m^a \end{bmatrix}, \quad \boldsymbol{\phi}_s = \begin{bmatrix} \phi_1^s \\ \phi_2^s \\ \vdots \\ \phi_m^s \end{bmatrix},$$

$$\boldsymbol{\Omega} = \begin{bmatrix} \omega_1 & & & \\ & \omega_2 & & \\ & & \ddots & \\ & & & \omega_n \end{bmatrix}, \quad \boldsymbol{\varsigma} = \begin{bmatrix} \zeta_1 & & & \\ & \zeta_2 & & \\ & & \ddots & \\ & & & \zeta_n \end{bmatrix}, \tag{11}$$

where ζ_j is the damping ratio of jth vibration mode of the structure. Eq. (7) is the state-space equation of the beam model.

3. Energy-based approach for optimal design

In this section, energy-based consideration [9] for the linear dynamic model, i.e., Eq. (7), is taken into account. The most attractive methodology that accounts for transient vibration responses is characterized by the maximization of the dissipation energy extracted by the feedback control system.

When a constant negative velocity feedback is considered the input control vector can be expressed as follows:

$$\mathbf{V}_a = -\mathbf{G}_s\dot{\boldsymbol{\phi}}_s = -\mathbf{G}\overline{\mathbf{C}}\dot{\boldsymbol{\chi}}, \tag{12}$$

where $\mathbf{G}$ is the feedback gain matrix. The corresponding closed-loop state-space equation is

$$\dot{\boldsymbol{\chi}} = \mathbf{A}\boldsymbol{\chi}, \tag{13}$$

where the closed-loop system matrix $\mathbf{A}$ is given by

$$\mathbf{A} = \begin{bmatrix} \mathbf{0}_{n\times n} & \mathbf{I}_{n\times n} \\ -\boldsymbol{\Omega}^2 & -\tilde{\mathbf{B}}\mathbf{G}\tilde{\mathbf{C}} - 2\boldsymbol{\varsigma}\boldsymbol{\Omega} \end{bmatrix},$$

where $\tilde{\mathbf{B}}$, $\tilde{\mathbf{C}}$, $\boldsymbol{\Omega}$, and $\boldsymbol{\varsigma}$ are defined in Eqs. (9) and (11).

The objective of optimization is to maximize the energy dissipated by the active controller. The more the energy dissipated by the control system, the less the energy is stored in the system. This can be used to simultaneously optimize the geometry of S/As and the values of feedback gains. The integrated total energy stored in the system can be written as

$$W = \int_0^\infty \boldsymbol{\chi}^{\mathrm{T}}\tilde{\mathbf{Q}}\boldsymbol{\chi}\,\mathrm{d}t, \tag{14}$$

where $\tilde{\mathbf{Q}}$ is defined as

$$\tilde{\mathbf{Q}} = \begin{bmatrix} \boldsymbol{\Omega}^2 & \mathbf{0} \\ \mathbf{0} & \mathbf{I}_{n\times n} \end{bmatrix}.$$

The application of the standard state transformation techniques to Eq. (14) yields

$$W = -\boldsymbol{\chi}^{\mathrm{T}}(t_0)\mathbf{P}\boldsymbol{\chi}(t_0), \tag{15}$$

where $\boldsymbol{\chi}(t_0)$ is the initial state and $\mathbf{P}$ is the solution of the following Lyapunov equation:

$$\mathbf{A}^{\mathrm{T}}\mathbf{P} + \mathbf{P}\mathbf{A} = \tilde{\mathbf{Q}}. \tag{16}$$

Thus, the problem can be expressed as a nonlinear optimization problem with constraints

$$\begin{aligned} &\text{Minimize} && J(\vec{\mathbf{X}}, \mathbf{G}, \vec{\mathbf{L}}) \\ &\text{subject to} && 0 \leqslant x_{i1}, x_{i2} \leqslant L_b, x_{i1} - x_{i2} \leqslant 0, G_{ij} \leqslant G_u \quad (i,j = 1,2,\ldots,m), \\ &&& x_{i2} - x_{(i+1)1} \leqslant 0 \quad (i = 1,2,\ldots,m-1), \end{aligned} \tag{17}$$

where $x_{i1} = x_i - L_i/2$, $x_{i2} = x_i + L_i/2$, $\vec{\mathbf{X}}$ is the vector of the m location variables x_i, $\vec{\mathbf{L}}$ is the vector of the m size variables L_i, G_u is the upper bound of the feedback control gains and $G_{ij} \in \mathbf{G}$.

4. General formulation for integer-real-encoded GAs

GAs have recently been recognized as a promising tool for numerical optimization of structural design problems. They are highly parallel, guided random, adaptive search techniques which were originally derived from the Darwinian evolutionary principle of "survival-of-the-fittest". They are superior to the traditional optimization methods based on gradient of the objective function as the search is not biased toward locally optimal solutions.

Since GAs can be directly used for unconstrained problems only, our optimal design problem needs to be transformed into an unconstrained problem by introducing the exterior penalty functions. Mathematically, the evaluation of the objective function can be represented by $\phi(\vec{\mathbf{X}}, \mathbf{G}, \vec{\mathbf{L}})$ in the following form:

$$\phi(\vec{\mathbf{X}}, \mathbf{G}, \vec{\mathbf{L}}) = J(\vec{\mathbf{X}}, \mathbf{G}, \vec{\mathbf{L}}) + \left(\sum_{i=1}^{m} r_i [\min\{0, (x_{i2} - x_{i1})\}]^2 + \sum_{i=1}^{m-1} r_i [\min\{0, (x_{(i+1)1} - x_{i2})\}]^2 \right), \quad (18)$$

where r_i is the penalty parameter. When $r_i \to \infty$, the solution of Eq. (18) tends to be the solution of the original problem defined in Eq. (17).

In this study, assume that a series of piezoelectric patches with standard sizes provided by the manufacturers are used for the optimal control. The patch pool can be defined as a set of patch sizes as $\mathbf{S} = \{S_k\}$ $(k = 0, 1, \ldots, p-1)$, in which there are p types of patch available for selection. The size variables are hence discrete and the resulting optimization problem is a discrete–continuous problem, which is difficult for the conventional optimization methods to solve. Thus, an integer–real-encoded GA is developed and implemented.

The fundamental mechanisms leading the GA search process are the equivalents of natural selection, crossover and mutation. GA deals with a population that is a collection of individuals and the chromosome of each individual represents a candidate solution. For any GA, a chromosome representation is needed to describe each individual in the population of interest. Each individual or chromosome is made up of a sequence of genes from a certain alphabet such as binary digits, floating point numbers, integers, etc. Michalewicz [14] has done extensive experimentation comparing real-encoded and binary GA, and showed that the former is more efficient in terms of CPU time. He also showed that a real-encoded representation moves the problem closer to the problem representation which offers higher precision with more consistent results across replications.

A typical chromosome for the integer–real-encoded GA can be illustrated in Fig. 2, where the location and feedback gains variables are encoded with real numbers but the size variables are encoded with integers I_i $(i = 1, 2, \ldots, m)$, which denote the sequence number of the ith patch in

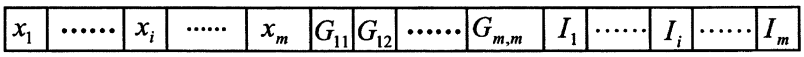

Fig. 2. A typical chromosome in integer–real-encoded GA.

the patch pool. The range of I_i is $[0, p-1]$ and the size of the ith patch is S_{I_i}. In this study, different genetic operators, i.e., mutation and crossover, are employed for the real- and integer-encoded parts of one chromosome, respectively. The uniform mutation and the whole arithmetical crossover are adopted for the real-encoded part. Let a_i and b_i be the lower and upper bounds, respectively, for the ith design variable. Uniform mutation sets the new variable value equal to $U(a_i, b_i)$, which is a random number uniformly distributed between a_i and b_i. The whole arithmetical crossover produces two complimentary linear combinations of the parents as

$$\tilde{X} = r\overline{X} + (1-r)\overline{Y},$$

$$\tilde{Y} = (1-r)\overline{X} + r\overline{Y},$$

where $r = U(0,1)$, $\overline{X}$ and $\overline{Y}$ are the parents, and $\tilde{X}$ and $\tilde{Y}$ are the offspring.

The mutation and crossover for the integer-encoded part are similar with the standard binary-encoded GA. The only difference is that the base of the integer-encoded GA is p.

5. Numerical example

In this section, based on the model and optimization criterion proposed above, an illustrative example of a simply supported beam is presented here to demonstrate the feasibility and effectiveness of the proposed method for optimal vibration control. The characteristic data of the beam are listed in Table 1 [13]. In the following design, the first four vibration modes are considered to be the controlled modes. The initial conditions of the generalized coordinate vector are given by

$$\boldsymbol{\eta}(0)^{\mathrm{T}} = [0 \quad 0 \quad 0 \quad 0],$$

$$\dot{\boldsymbol{\eta}}(0)^{\mathrm{T}} = [0.2 \quad 0.4 \quad 0.6 \quad 0.8]$$

to make the first four vibration modes have roughly equivalent kinetic energy stored in the system if no control applied.

Table 1
Structure and piezoelectric patch specifications

Item	Beam	Actuators	Sensors
Mass density (kg/m^3)	1190	1800	1800
Young's modulus (GPa)	3.1028	2	2
Poisson's ratio	0.3	0.3	0.3
Piezoconstant d_{31} (m/V)		2.3×10^{-11}	2.3×10^{-11}
Piezoconstant h_{31} (V/m)			4.32×10^{8}
Thickness (m)	1.6×10^{-3}	4×10^{-5}	4×10^{-5}
Length (m)	0.5		
Width (m)	0.01		
Damping ratio	0.01		

For a simply supported beam, the normalized modal shape can be expressed as $U_j(x) = \sqrt{(2/(\rho_b A_b L))}\sin(j\pi x/L)$, and the natural frequency is $\omega_j = (j^2\pi^2/L^2)\sqrt{E_b J_b/(\rho_b A_b)}$, where $j = 1, 2, \ldots, n$.

The optimization problem as previously formulated is a nonlinear optimization with constraints. In this case, besides the geometric constraints, a simple bound is imposed on the feedback control gain matrix $\mathbf{G}$, i.e., $0 < G_{ij} \leqslant 0.4$. In order to ensure the system to be asymptotically stable, an additional constraint is needed, i.e., $\det(\mathbf{G}) > 0$, where $\det(\mathbf{G})$ represents the determinant of the matrix $\mathbf{G}$.

The GA control parameters are as follows. The population size, the crossover probability, the mutation probability, and the maximum number of generations are set as 200, 0.8, 0.05 and 300, respectively.

5.1. Results of transient response control

In this case, the patch pool is defined as $S_k = 0.05(k+1), k = 0, 1, \ldots, 9$. To control the transient response of the simply supported beam, three cases with one to three pieces of piezoelectric patch have been studied. In these cases, the responses of the beam are obtained by the superposition of the first four vibration modes. Thus, the transient response control of the beam implies the simultaneous control of the first four vibration modes. The optimization results are shown in Table 2. The time behaviors of the vibration modes with and without control using one to three pieces of piezoelectric patch are shown in Figs. 3–6. From Table 2 and Figs. 3–6, it is apparent that the speed of decay of the vibration increases when more patches are used. This implies that the vibration of the structure can be controlled more effectively by using more patches, with the optimized placement and size, as well as the optimized feedback control gains.

5.2. Results of optimal control of specific vibration modes

In order to investigate the optimal distribution of the piezoelectric patches for specific vibration modes, two cases, Case 1 to consider one specific vibration mode and Case 2 to consider the first

Table 2
Optimal placement and size of S/As and feedback gain

Number of patches m	Placement and size of patches $x_i(L_i)$ (m)	Feedback gain matrix	Objective Function $\boldsymbol{\phi}(\vec{\mathbf{X}}, \mathbf{G}, \vec{\mathbf{L}})$
1	0.0768 (0.1)	[0.4]	0.1922
2	0.0750 (0.1) 0.3544 (0.15)	$\begin{bmatrix} 0.4 & 0.4 \\ 0 & 0.4 \end{bmatrix}$	0.1634
3	0.0792 (0.1) 0.1793 (0.1) 0.4138 (0.15)	$\begin{bmatrix} 0.4 & 0 & 0 \\ 0 & 0.4 & 0.0342 \\ 0 & 0 & 0.4 \end{bmatrix}$	0.1388

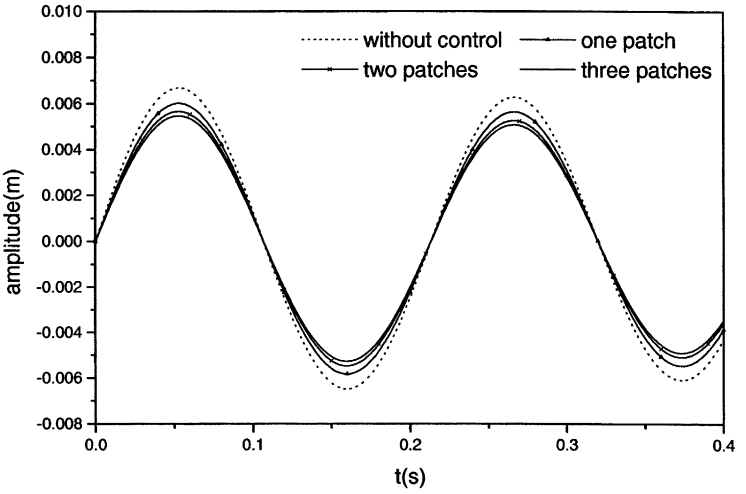

Fig. 3. Time response of 1st mode with different number of patches.

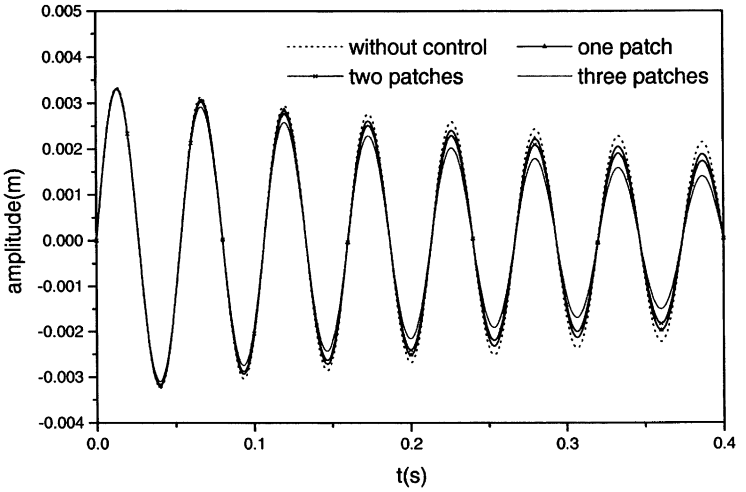

Fig. 4. Time response of 2nd mode with different number of patches.

several vibration modes simultaneously, have been investigated. In these cases, the feedback control gain matrix **G** is set as a constant 0.4 to emphasize the optimal distribution of the piezoelectric patches. Moreover, the sizes of the patches are not confined to a patch pool. Instead, they are continuous variables.

Case 1: *To consider one specific vibration mode*: The optimal geometric distributions of the piezoelectric patches are shown in Table 3. It can be found from Table 3 that, for one specific vibration mode, no matter how many piezoelectric patches are used, the optimal distributions of the piezoelectric patches should be located within the regions separated by the vibration nodal

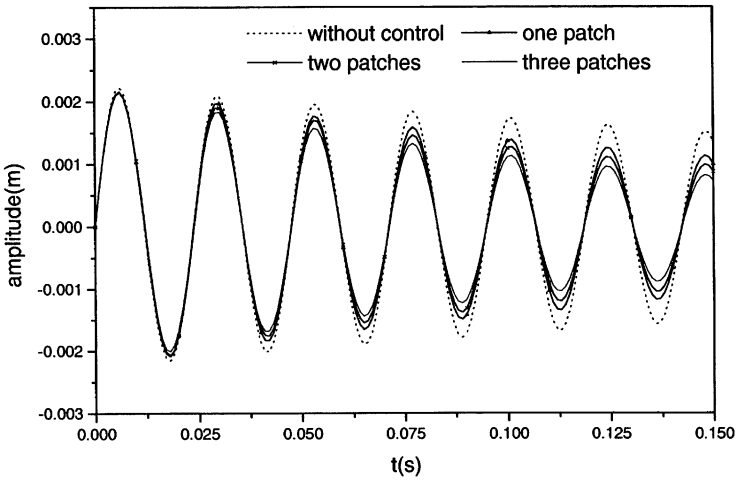

Fig. 5. Time response of 3rd mode with different number of patches.

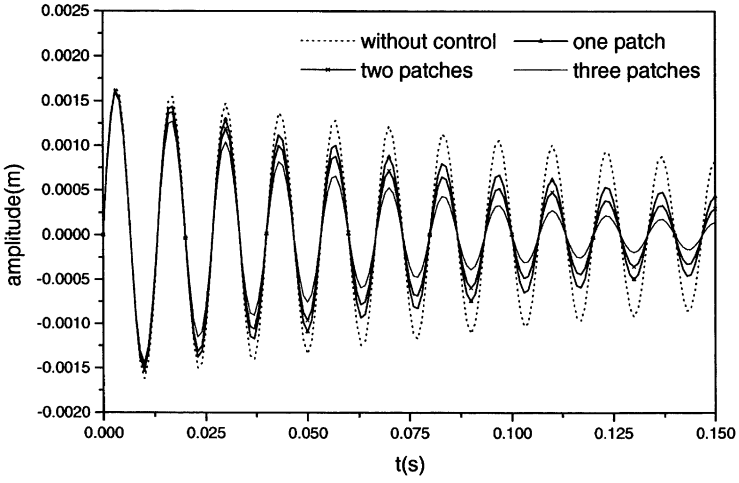

Fig. 6. Time response of 4th mode with different number of patches.

lines. Furthermore, there exists a cut-off number of patches for one specific mode. If more patches are used compared with this number, the control performance can only be improved slightly. Actually, this cut-off number equals to the number of regions separated by the vibration nodal line(s) of this mode. The cut-off numbers of patches for the 1st, 2nd, 3rd, and 4th vibration modes are 1, 2, 3, and 4, respectively.

The observation that piezoelectric patches should be separated by nodal lines may be physically explained by the following two points. First, if a piezoelectric sensor is located across the nodal line, the output voltage will decrease because the two sides of the nodal line will generate opposite charges over the sensor which counteract each other. Thus, the sensor signal fed back to the

Table 3
Optimal placement and size of S/As for unique vibration mode

Patch	Mode							
	1st		2nd		3rd		4th	
	$x_{i1}-x_{i2}$ (m)	ϕ	$x_{i1}-x_{i2}$ (m)	ϕ	$x_{i1}-x_{i2}$ (m)	ϕ	$x_{i1}-x_{i2}$ (m)	ϕ
1	0.0645−0.4355	0.0533	0.2822−0.4678	0.0439	0.1882−0.3118	0.0373	0.1411−0.2339	0.0324
2	0.0678−0.3966	0.0530	0.0322−0.2178	0.0324	0.0215−0.1452	0.0257	0.0161−0.1088	0.0213
	0.3966−0.4670		0.2822−0.4678		0.3548−0.4785		0.2661−0.3588	
3	0.0375−0.1190	0.0527	0.0322−0.2178	0.0322	0.0215−0.1452	0.0196	0.0161−0.1088	0.0158
	0.1190−0.3814		0.2834−0.4547		0.1882−0.3118		0.1411−0.2338	
	0.3814−0.4626		0.4547−0.4854		0.3548−0.4785		0.3911−0.4839	
4	0.0280−0.0864	0.0526	0.0334−0.2046	0.0320	0.0227−0.1305	0.0195	0.0161−0.1089	0.0126
	0.0864−0.1553		0.2046−0.2353		0.1305−0.1552		0.1411−0.2339	
	0.1553−0.3769		0.2674−0.3046		0.1882−0.3118		0.2661−0.3589	
	0.3769−0.4613		0.3046−0.4659		0.3548−0.4785		0.3911−0.4839	
5	0.0258−0.0794	0.0525	0.0189−0.6000	0.0317	0.0132−0.0421	0.0194	0.0161−0.1089	0.0126
	0.0794−0.1407		0.6000−0.1907		0.0421−0.1437		0.1354−0.1583	
	0.1407−0.3765		0.1907−0.2313		0.1782−0.2028		0.1583−0.2327	
	0.3765−0.4298		0.2673−0.3043		0.2028−0.3106		0.2661−0.3589	
	0.4298−0.4770		0.3043−0.4659		0.3548−0.4785		0.3911−0.4839	
6	—	—	0.0183−0.0578	0.0317	0.0225−0.1336	0.0192	0.0170−0.0984	0.0125
			0.0578−0.2004		0.1336−0.1560		0.0984−0.1165	
			0.2004−0.2341		0.1791−0.2063		0.1411−0.2339	
			0.2622−0.2874		0.2063−0.2938		0.2670−0.3480	
			0.2874−0.3138		0.2938−0.3209		0.3480−0.3664	
			0.3138−0.4654		0.3548−0.4785		0.3911−0.4839	
7	—	—	—	—	—	—	0.0093−0.0296	0.0124
							0.0296−0.0953	
							0.0953−0.1156	
							0.1336−0.1522	
							0.1522−0.2330	
							0.2661−0.3589	
							0.3911−0.4839	

actuator will decrease or even become nil. Accordingly, the control force generated by the actuator will become smaller and the control effect will be impaired. Second, at both sides of the nodal line, the structure vibrates at opposite directions. If a piezoelectric actuator is located across

Table 4
Optimal placement and size of S/As for combined vibration mode

Patch	Modes							
	1st		1st and 2nd		1st, 2nd, and 3rd		1st, 2nd, 3rd, and 4th	
	$x_{i1}-x_{i2}$ (m)	ϕ	$x_{i1}-x_{i2}$ (m)	ϕ	$x_{i1}-x_{i2}$ (m)	ϕ	$x_{i1}-x_{i2}$ (m)	ϕ
1	0.0645−0.4355	0.0533	0.0349−0.2442	0.1049	0.0245−0.1730	0.1500	0.0190−0.1354	0.1911
2	0.0678−0.3966	0.0530	0.0364−0.2500	0.0873	0.0251−0.1797	0.1238	0.0194−0.1407	0.1560
	0.3966−0.4670		0.2500−0.4636		0.3203−0.4749		0.3590−0.4805	
3	0.0375−0.1190	0.0527	0.0381−0.2137	0.0857	0.0275−0.1810	0.1090	0.0207−0.1375	0.1364
	0.1190−0.3814		0.2137−0.2865		0.1810−0.3206		0.1375−0.2592	
	0.3814−0.4626		0.2865−0.4619		0.3206−0.4724		0.3484−0.4795	
4	0.0280−0.0864	0.0526	0.0384−0.1937	0.0852	0.0278−0.1663	0.1066	0.0223−0.1422	0.1229
	0.0864−0.1553		0.1937−0.2500		0.1663−0.2490		0.1422−0.2504	
	0.1553−0.3769		0.2500−0.3063		0.2490−0.3332		0.2504−0.3580	
	0.3769−0.4613		0.3063−0.4616		0.3332−0.4722		0.3580−0.4775	
5	0.0258−0.0794	0.0525	0.0222−0.0717	0.0848	0.0283−0.1511	0.1052	0.0225−0.1354	0.1203
	0.0794−0.1407		0.0717−0.1944		0.1511−0.2094		0.1354−0.2184	
	0.1407−0.3765		0.1944−0.2505		0.2094−0.2907		0.2184−0.2812	
	0.3765−0.4298		0.2505−0.3067		0.2907−0.3491		0.2812−0.3647	
	0.4298−0.4770		0.3067−0.4616		0.3491−0.4717		0.3647−0.4774	
6	—	—	0.0223−0.0717	0.0844	0.0283−0.1415	0.1046	0.0226−0.1239	0.1187
			0.0717−0.1941		0.1415−0.1914		0.1239−0.1706	
			0.1941−0.2500		0.1914−0.2496		0.1706−0.2492	
			0.2500−0.3059		0.2496−0.3083		0.2492−0.3260	
			0.3059−0.4283		0.3083−0.3584		0.3260−0.3752	
			0.4283−0.4778		0.3584−0.4717		0.3752−0.4772	
7	—	—	—	—	0.0172−0.0560	0.1041	0.0228−0.1166	0.1175
					0.0560−0.1449		0.1166−0.1639	
					0.1449−0.1945		0.1639−0.2256	
					0.1945−0.2540		0.2256−0.2746	
					0.2540−0.3104		0.2746−0.3358	
					0.3104−0.3597		0.3358−0.3837	
					0.3597−0.4718		0.3837−0.4771	

the nodal line, the control force generated by the actuator will suppress the vibration on one side, but accelerate the vibration on the other side. Thus the entire control effect contributed by the control force is weakened.

Case 2: *To consider the first several vibration modes simultaneously*: The optimal geometric distributions of the piezoelectric patches are shown in Table 4. It can be found from Table 4 that, when the number of piezoelectric patches used is identical with the number of regions separated by the nodal lines of all these vibration modes, the optimal distributions of the patches should be located within these regions. For example, if 1, 2, 4, and 6 pieces of patch are used for the 1st, the 1st and 2nd, the 1st, 2nd, and 3rd, and the 1st, 2nd, 3rd, and 4th vibration modes, respectively, the optimal distributions of the patches are located within the regions separated by the nodal lines. It can be schematically shown in Fig. 7, in which the dashed lines denote the nodal lines of the vibration modes and the areas filled with diagonal lines represent the piezoelectric patches bonded on the beam.

However, for other numbers of patches used, it does not comply with this rule. The explanation is as follows. As some vibration modes are controlled simultaneously, although it will weaken the control effect for certain vibration modes if one patch is located across the nodal line of this mode, it will possibly improve the control effect for the other vibration modes which have no nodal line across the patch area. Thus, the overall control effect may still be improved and the optimal distributions of the piezoelectric patches can be located across some nodal lines.

The two observations can be summarized as: (1) for one specific vibration mode, the optimal distributions of piezoelectric patches should be located within the regions separated by the nodal lines of this mode; and (2) for several combined vibration modes, if the number of patches is

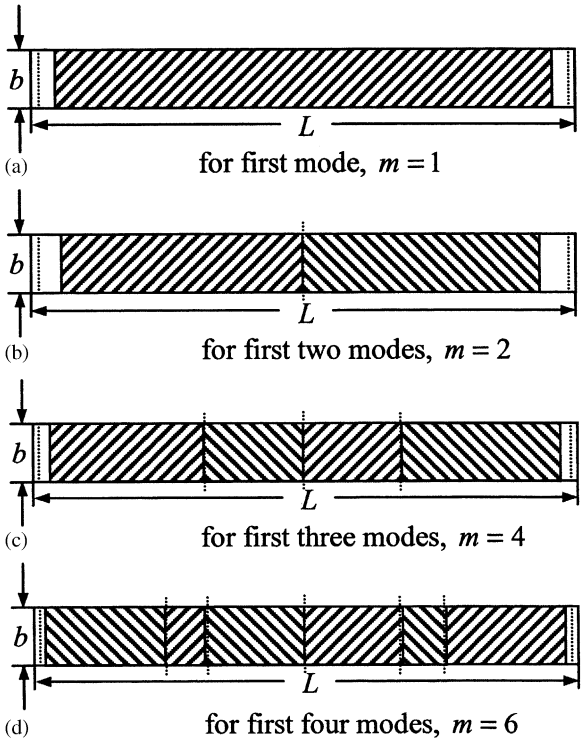

Fig. 7. Optimal geometric distributions of piezoelectric patches for specific vibration modes of simply supported beam.

identical with the number of regions separated by the nodal lines of all these modes, the optimal distributions of the patches should also be located within these regions. Although the above findings are obtained from computational results and difficult to be demonstrated analytically, they provide some meaningful knowledge and guidelines for practical design.

6. Conclusions

In this paper, the integrated optimization design of the vibration control system, including the placement and size of the piezoelectric patches, as well as the feedback control gains has been formulated. An integer–real-encoded GA has been developed to solve this discrete–continuous optimization problem. The energy dissipation method has been adopted for the vibration suppression of the structure. The results of a simply supported beam show that using this integrated optimization of geometric distribution of the piezoelectric patches and the feedback control gains, the vibration of the structure can be effectively suppressed. It can be concluded that when more pieces of patch are applied, the control effect can be improved. Furthermore, for optimal vibration control of one specific vibration mode, the optimal distributions of the piezoelectric patches should be located within the regions separated by the vibration nodal lines, and for several combined vibration modes, only when the number of piezoelectric patches used is identical with the number of regions separated by the nodal lines of all these modes, the optimal distributions of the patches are located within these regions.

References

[1] E.F. Crawley, J. de Luis, Use of Piezoelectric actuators as elements of intelligent structures, *AIAA Journal* 25 (1987) 1373–1385.
[2] A. Baz, S. Poh, Performance of an active control system with piezoelectric actuators, *Journal of Sound and Vibration* 126 (1988) 327–343.
[3] S. Devasia, T. Meressi, B. Paden, E. Bayo, Piezoelectric actuator design for vibration suppression: placement and sizing, *Journal of Guidance, Control, and Dynamics* 16 (1993) 859–864.
[4] A.K. Dhingra, B.H. Lee, Optimal placement of actuators in actively controlled structures, *Engineering Optimization* 23 (1994) 99–118.
[5] A. Arbel, Controllability measures and actuator placement in oscillatory systems, *International Journal of Control* 33 (1981) 565–574.
[6] A. Hac, L. Liu, Sensor and actuator location in motion control of flexible structures, *Journal of Sound and Vibration* 167 (1993) 239–261.
[7] A.K. Dhingra, B.H. Lee, Multiobjective design of actively controlled structures using a hybrid optimization method, *International Journal for Numerical Methods in Engineering* 38 (1995) 3380–3401.
[8] S. Kondoh, C. Yatomi, K. lnoue, The positioning of sensors and actuators in the vibration control of flexible systems, *JSME International Journal Series 3* 33 (1992) 145–152.
[9] A.C. Lee, S.T. Chen, Collocated sensor/actuator positioning and feedback design in the control of flexible structure system, *Journal of Vibration and Acoustics* 116 (1994) 146–154.
[10] Z.D. Wang, S.H. Chen, W.Z. Han, Integrated structural and control optimization of intelligent structures, *Engineering Structures* 21 (1999) 183–191.
[11] I. Lee, J.H. Han, Optimal placement of piezoelectric actuators in intelligent structures using genetic algorithms, *Third ICIM/ECSSM '96*, 1996, pp. 872–875.

[12] H.W. Zhang, B. Lennox, P.R. Goulding, A.Y.T. Leung, A float-encoded genetic algorithm technique for integrated optimization of piezoelectric actuator and sensor placement and feedback gains, *Smart Materials and Structures* 9 (2000) 552–557.
[13] H.S. Tzou, *Piezoelectric Shells: Distributed Sensing and Control of Continua*, Kluwer Academic Publishers, Dordrecht, 1993.
[14] Z. Michalewicz, *Genetic Algorithms + Data Structures = Evolution Programs*, AI Series, Springer, New York, 1994.